Journal of Sound and Vibration (2000) **233**(4), 707–726
doi:10.1006/jsvi.1999.2839, available online at http://www.idealibrary.com on IDEAL®

COMPARISON OF SEVERAL STRATEGIES IN THE ACTIVE STRUCTURAL ACOUSTIC CONTROL USING STRUCTURAL STRAIN MEASUREMENTS

P. MASSON AND A. BERRY

G.A.U.S, Mechanical Engineering Department, Université de Sherbrooke, Sherbrooke, Québec, Canada J1K 2R1

(*Received* 21 *January* 1999, *and in final form* 16 *December* 1999)

Two optimized approaches are herein proposed to lighten the real-time computation of the radiated acoustic power from planar structures using discrete strain measurements. These approaches are compared to a reference approach involving finite differences reconstruction of the displacement field from the strain field. The first optimized approach allows the direct calculation of the radiated acoustic power from the discrete strain field while the second optimized approach employs an accelerated evaluation of the radiated acoustic power based on a wavelet transform of the displacement field. The evaluation of the radiated acoustic power from discrete strain values is experimentally assessed using the reference finite differences approach and both optimized approaches. Piezoelectric film (PVDF) strain sensors are used for this validation as well as a feedforward filtered-X LMS controller. Details on the real-time implementation of the cost functions are presented, especially on the off-line adaptation of the control filter. Formal comparisons using acoustic and vibration measurements are presented to better illustrate the control performance and mechanism of the different approaches. Experimental results serve to demonstrate the interest of using the optimized approaches as compared to the reference approach and it is shown that a significant gain in computational burden can be obtained using the proposed optimized approaches without sacrificing the control performance.

1. INTRODUCTION

The development of high-performance dedicated signal processors has driven the interest for active noise control in recent years. These processors are now more compact and a variety of tools exists to easily implement numerical controllers on them.

It is well known that passive methods involving foams, viscoelastic layers and other absorbing or dissipative materials cannot be used efficiently to reduce low-frequency noise. To perform noise control at those frequencies, different active control strategies have been proposed and can be distinguished as active noise control (ANC) [1] and active structural acoustic control (ASAC) [2]. While active noise control requires the use of actuators located in the acoustic field, i.e., loudspeakers, the active structural acoustic control allows for the integration of both the error sensors and the actuators in the structure itself, following the trend towards smart materials. Moreover, it has been shown that, most of the time, ASAC has a lower requirement on the number of secondary sources needed to perform the control as compared to ANC [1].

Among the active structural acoustic control strategies, global and local strategies can be distinguished. Local control refers to spatially localized control (zones of silence) while global control is associated with extended control effect using cost functions closely related

0022-460X/00/240707 + 20 $35.00/0

to energy quantities [3]. In this respect, the information given by the error sensors was used in the definition of cost functions based, for example, either on the farfield pressure in prescribed directions [4–6], the volume velocity [7, 8] or the radiated acoustic power [9, 10]. The latter appears to be very promising as it ensures global control and, moreover, if working in the wavenumber domain [11, 12], allows for proper concentration of the control effort in the supersonic region of the structural displacement wavenumber spectrum, where the radiating wavenumber components are located.

The control strategy based on the radiated acoustic power and defined in the wavenumber domain first requires the wavenumber transformation of the displacement (or acceleration) field of the structure. The supersonic (radiating) components of the spectrum can then be identified and minimized. For this purpose, as compared to spatially extended sensors [13, 14], discrete sensors are more appropriate as they allow to distinguish between the structural components on two-dimensional structures [4]. Moreover, following the trend towards smart materials, strain sensors appear to be well suited for integration into structures and materials. As they do not measure directly the displacement or acceleration of the structure, the use of these sensors implies an additional step for the estimation of the radiated acoustic power. Therefore, there is a need to reduce the computational burden associated with the use of such sensors.

This paper is thus concerned with the experimental validation of two optimized approaches which are herein proposed to evaluate the radiated acoustic power from discrete strain measurements. The cost function is defined as global and is expressed as the radiated acoustic power in the wavenumber domain and using discrete strain sensors. The first optimized approach allows the calculation of the radiated acoustic power *directly* from the strain field, without requiring any reconstruction of the displacement field. This first approach is based on a double integration by parts of the radiated acoustic power integral to provide an estimate in terms of the wavenumber transform of the *strain* field. The second optimized approach is directed towards the acceleration of the radiated acoustic power calculation by using a *wavelet transform* of a reconstructed displacement field, thus replacing both the Fourier transform and the integration of the radiating components [15]. In this second approach, the wavelet transform is chosen because it can have efficient restriction on the supersonic region using a single space-wavenumber transformation. It is known that the wavelet transform has the property to localize the energy both in a given region of the wavenumber spectrum and spatially on the structure. The approach presented in this paper thus benefits from the wavelet framework, even if the analysis is herein restricted to the wavenumber localization in order to simplify the illustration of the approach.

The reference approach based on a finite differences reconstruction of the displacement field is first briefly presented. Both optimized approaches are then presented and their control performance is experimentally compared to the reference approach.

2. ACOUSTIC RADIATION IN THE WAVENUMBER DOMAIN

For the sake of illustration, the acoustic radiation from a baffled rectangular thin beam is considered in this work. The acoustic pressure $p(M)$ radiated at a point M from a baffled beam can be expressed by the Rayleigh's integral:

$$p(M) = \frac{\rho_0}{2\pi} \int_A \ddot{W}(P, t) \frac{e^{-ikr}}{r} dA, \tag{1}$$

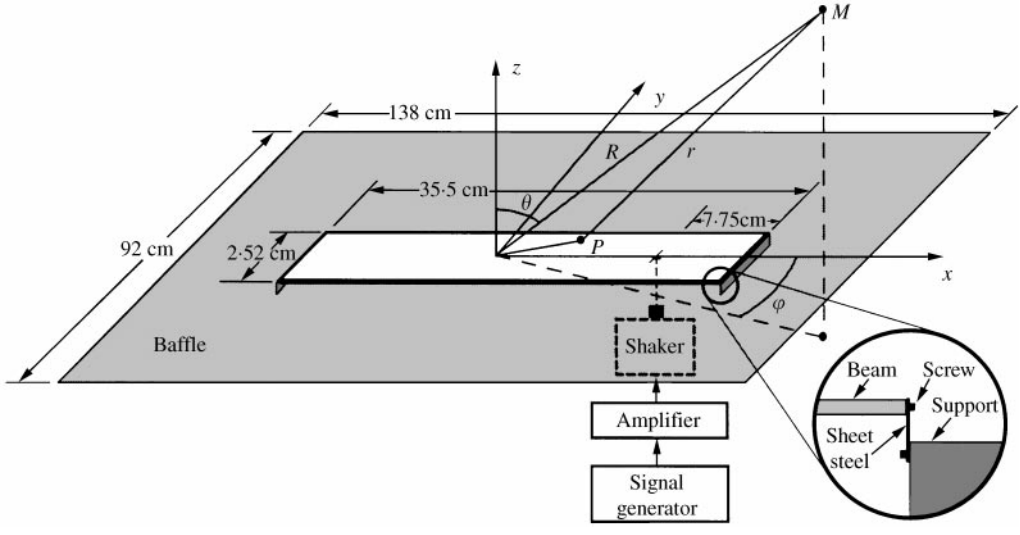

Figure 1. Experimental set-up: the baffled beam.

where ρ_0 is the mass density of the fluid, $\ddot{W}(P, t)$ is the beam transverse acceleration at a point P, k is the acoustic wavenumber in the fluid, r is the distance between P and M and A is the surface of the beam, as presented in Figure 1. Assuming harmonic and constant displacement along the y direction such that $W(P, t) = w(x)e^{i\omega_0 t}$, the previous equation can be used to obtain a farfield approximation of the radiated acoustic pressure [16]:

$$p(R, \phi, \varphi) = -\frac{\omega_0^2 \rho_0}{2\pi} \frac{e^{-ikR}}{R} \tilde{w}(\lambda, \mu), \tag{2}$$

where

$$\lambda = k \sin\theta \cos\varphi, \qquad \mu = k \sin\theta \sin\varphi \tag{3, 4}$$

and where R, θ and φ are the spherical co-ordinates of the point M. $\tilde{w}(\lambda, \mu)$ is the double wavenumber transform of the beam displacement, analogous to the inverse Fourier transform defined, for a beam of finite width assuming constant displacement along the y direction, as [7]

$$\tilde{w}(k_x, k_y) = \int_{-l_x}^{l_x} \int_{-l_y}^{l_y} w(x, y) e^{i(k_x x + k_y y)} \, dy \, dx \tag{5}$$

$$= \frac{2 \sin k_y l_y}{k_y} \int_{-l_x}^{l_x} w(x) e^{-ik_x x} \, dx \tag{6}$$

$$= \frac{2 \sin k_y l_y}{k_y} \tilde{w}(k_x), \tag{7}$$

where l_x is the half-length of the beam, l_y is the halfwidth of the beam and k_x and k_y are, respectively, the x and y components of the structural wavenumber.

The acoustic power Π radiated from the beam can be expressed as the integral over a hemisphere of the mean square of the sound pressure in the far field:

$$\Pi = \frac{1}{2\rho_0 c} \int_S |p(R, \theta, \varphi)|^2 \, \mathrm{d}S, \tag{8}$$

where S is the surface of the hemisphere and c is the speed of sound in the fluid.

In order to exploit the physical mechanisms of structural radiation, the radiated acoustic power is expressed in the wavenumber domain [11, 17, 14]. The radiated acoustic power in the wavenumber domain is obtained by substituting equation (2) into equation (8), as presented in detail in reference [18]:

$$\Pi = \frac{\rho_0 \omega_0^3}{8\pi^2} \int_{-k}^{k} \int_{-\sqrt{k^2-\lambda^2}}^{\sqrt{k^2-\lambda^2}} \frac{|\tilde{w}(\lambda, \mu)|^2}{\sqrt{k^2 - \lambda^2 - \mu^2}} \, \mathrm{d}\mu \, \mathrm{d}\lambda. \tag{9}$$

In equation (9), the integration is performed over the supersonic region of the structural wavenumber spectrum (i.e., the region where the acoustic wavenumber k is larger than the structural wavenumber given by $\sqrt{\lambda^2 + \mu^2}$), which shows that only supersonic structural waves radiate sound in the far field. The minimization of the displacement wavenumber spectrum (weighted by $(1/\sqrt{k^2 - \lambda^2 - \mu^2})$ in the supersonic region will then minimize the radiated acoustic power.

For a narrow beam (for which $|k_y l_y| \ll 1$) and using equations (2) and (7), equation (9) reduces to the form

$$\Pi_{finite} = \frac{\rho_0 \omega_0^3 l_y^2}{2\pi} \int_{-k}^{k} |\tilde{w}(\lambda)|^2 \, \mathrm{d}\lambda. \tag{10}$$

The objective of the following control approaches is to derive cost functions from structural strain measurements which approximate the exact radiated acoustic power given by equation (10).

3. APPROACHES FOR USING STRAIN MEASUREMENTS IN THE EVALUATION OF THE RADIATED ACOUSTIC POWER

Three approaches are herein presented for using strain measurements in the evaluation of the radiated acoustic power, through equation (10). The first approach, based on a finite differences scheme for the reconstruction of the displacement field from the strain field, is referred to as the reference approach because it involves fewer assumptions than other approaches. Two optimized approaches are also presented: the first one is based on rewriting equation (10) in terms of the wavenumber transform of the strain field; the second one is based on a wavelet approximation of the radiated acoustic power.

In the following, it will be assumed that the Bernoulli thin beam conditions apply, i.e., the strain $\varepsilon_x(x)$ at the surface of the beam is related to the second space derivative, in that direction, of the displacement field $w(x)$:

$$\varepsilon_x(x) = -\frac{h_b}{2} \frac{\partial^2 w(x)}{\partial x^2}, \tag{11}$$

where h_b is the thickness of the beam.

3.1. REFERENCE APPROACH: FINITE DIFFERENCES SCHEME

A finite differences scheme can be used to reconstruct the displacement field $w(x)$ from the discrete strain field $\partial^2 w(x)/\partial x^2$ known on a p equally spaced grid of points on the beam (x_i) $(i = 1, 2, \ldots, p$, where $i = 1$ and $i = p$ are on edges) [10]. This scheme however requires the knowledge of two of the boundary conditions of the beam. The central-difference scheme can be written in a matrix form as

$$\mathbf{A}_{p,\,p+2}\,\mathbf{w}_{p+2} = \mathbf{w}_p'', \tag{12}$$

where the subscripts indicate the dimensions of the matrices or vectors. In this equation, $\mathbf{w}_p''$ is the vector of the measured strain and $\mathbf{w}_{p+2}$ is built from the displacement at each measurement point w_i and from the slopes of the displacement field in the x direction $w_j' \equiv \partial w(x_j)/\partial x$ on the edges such that

$$\mathbf{w}_{p+2} = \begin{bmatrix} w_1' \\ w_1 \\ w_2 \\ \vdots \\ w_p \\ w_p' \end{bmatrix}. \tag{13}$$

Indeed, it is seen that equtaion (12) can be solved only if two components of $\mathbf{w}_{p+2}$ are known *a priori*. These two components can be chosen from the first two components and the last two components of this vector, representing boundary conditions on the displacement or the slope along the $x = x_1$ and $x = x_p$ edges. In the following, four physical strain measurement points are used, in addition to two assumed strain values on the edges. Under these conditions and for a simply supported beam, taking into account the zero-strain condition $(w'' = 0)$ as well as the zero-displacement condition $(w = 0)$ on the edges, the finite differences scheme reduces to

$$\frac{1}{\Delta x^2}\begin{bmatrix} -2\Delta x & 2 & & & & & \\ & -2 & 1 & & & & \\ & 1 & -2 & 1 & & & \\ & & 1 & -2 & 1 & & \\ & & & 1 & -2 & 1 & \\ & & & & 2 & 2\Delta x \end{bmatrix}\begin{bmatrix} w_1' \\ w_2 \\ w_3 \\ w_4 \\ w_5 \\ w_6' \end{bmatrix} = \begin{bmatrix} 0 \\ w_2'' \\ w_3'' \\ w_4'' \\ w_5'' \\ 0 \end{bmatrix}, \tag{14}$$

where Δx is the space interval between two consecutive points and $w_k'' = \partial^2 w(x_k)/\partial x^2$ is the strain measured in the x direction.

The reconstructed displacement field obtained from the vector $\mathbf{w}_6$, by solving equation (14), and from the zero-displacement assumption on the edges, is then transformed using a discretized version of equation (6) given by

$$\tilde{w}(k_x) = \sum_{i=1}^{6} w_i \mathrm{e}^{\mathrm{i}k_x x_i}\Delta x \tag{15}$$

and substituted in equation (10) to obtain the radiated acoustic power.

In order to obey the Nyquist criterion, it is expected that two measurement points will be required per mechanical wavelength to obtain an adequate estimate of the radiated acoustic power. Therefore, four strain sensors along the beam, together with the two assumed zero-strain values at the beam edges, should allow an adequate estimate up to the third vibration mode. Spatial aliasing can impair the estimate of the radiated acoustic power as the precision obtained on the wavenumber components of the displacement field is directly related to the accuracy of the radiated acoustic power estimate. The use of zero padding can improve the accuracy of the estimate by providing a larger number of components in the evaluation of the radiation integral given in equation (10). Spatial aliasing was extensively studied before through numerical simulations [10].

3.2. OPTIMIZED APPROACHES

3.2.1. *Direct approach*

The first optimized approach aims at expressing the radiated acoustic power (equation (10)) directly in terms of the Fourier transform of the strain measurements. This approach is based on a double integration by parts of the wavenumber transform (equation (5)). The first integration by parts with respect to the x variable leads to the following result for the wavenumber transform:

$$\tilde{w}(k_x, k_y) = \frac{1}{\mathrm{i}k_z} \oint w(x, y) \mathrm{e}^{\mathrm{i}(k_x x + k_y y)} \mathbf{n} \cdot \mathbf{i} \, \mathrm{d}l - \frac{1}{\mathrm{i}k_x} \int_{-a}^{a} \int_{-b}^{b} \frac{\partial w(x, y)}{\partial x} \mathrm{e}^{\mathrm{i}(k_x x + k_y y)} \, \mathrm{d}y \, \mathrm{d}x, \quad (16)$$

where $\mathbf{i}$ is the unit vector in the x direction, $\mathbf{n}$ is the unit outer vector normal to an edge and $\oint$ denotes the integration over the contour of the surface. The second integration by parts with respect to the x variable gives

$$\tilde{w}(k_x, k_y) = \frac{1}{\mathrm{i}k_z} \oint w(x, y) \mathrm{e}^{\mathrm{i}(k_x x + k_y y)} \mathbf{n} \cdot \mathbf{i} \, \mathrm{d}l + \frac{1}{k_x^2} \oint \frac{\partial w(x, y)}{\partial x} \mathrm{e}^{\mathrm{i}(k_x x + k_y y)} \mathbf{n} \cdot \mathbf{i} \, \mathrm{d}l$$

$$- \frac{1}{k_x^2} \tilde{S}(k_x, k_y) \quad (17)$$

with

$$\tilde{S}(k_x, k_y) = \int_{-a}^{a} \int_{-b}^{b} \frac{\partial^2 w(x, y)}{\partial x^2} \mathrm{e}^{\mathrm{i}(k_x x + k_y y)} \, \mathrm{d}y \, \mathrm{d}x, \quad (18)$$

where $\tilde{S}(k_x, k_y)$ is the wavenumber transform of the strain field. Equation (17) can be rewritten as

$$\tilde{w}(k_x, k_y) = \sum_{i=1}^{2} I_i - \frac{1}{k_x^2} \tilde{S}(k_x, k_y), \quad (19)$$

where I_i are the subsisting boundary terms associated with edges $i = 1, 2$ parallel to the y-axis.

Preceding work has shown that, for a simply supported structure, the boundary terms can be neglected at low frequency without affecting significantly the radiated acoustic

power estimate [10]. It was observed that, for a given mode, the boundary term in equation (19) and the surface strain transform term in equation (18) are of the same order of magnitude, below the modal frequency. The importance of the surface strain-transform term increases slightly close to that frequency while its relative importance decreases rapidly above this frequency. The global effect is that, with an increase in frequency, more and more modes are considered in which the surface-strain transform term has little effect or, conversely, the boundary term has large relative effect. Therefore, for a simply supported beam and using four strain sensors, the following one-dimensional form of equation (19) can be used if $k_x \neq 0$:

$$\tilde{w}(k_x) \approx -\frac{1}{k_x^2} \sum_{i=1}^{4} w_i'' \mathrm{e}^{\mathrm{i}k_x x_i} \Delta x, \tag{20}$$

and if $k_x = 0$, the following form is used [10]:

$$\tilde{w}(0) \approx \sum_{i=1}^{4} \left(\frac{x_i^2}{2} - \frac{l_x^2}{2} \right) w_i'' \Delta x. \tag{21}$$

3.2.2. *Wavelet approach*

In the finite differences approach, the radiated acoustic power was related to the integration, in the supersonic region of the wavenumber domain, of the squared norm of the spectral components (corresponding to energy density) of the displacement field, as it appears in equation (10). The second optimized approach uses a space-wavenumber wavelet transform to *observe* the energy localized in the supersonic region. This approach has been theoretically investigated before [15] and a condensed presentation of the approach is only given here.

The wavelet transform of a function $f(x)$ is defined as

$$(W_\psi f)(b, a) = \frac{1}{\sqrt{|a|}} \int_{-\infty}^{\infty} f(x) \, \overline{\psi\left(\frac{x - b}{a} \right)} \, \mathrm{d}x, \tag{22}$$

where $\psi(x)$ is called the mother wavelet from which all the other wavelets are generated using a *translation* parameter b and a *dilation* parameter a. The overbar indicates the complex conjugate. It can be shown [19] that this wavelet transform gives localized information on a function $f(x)$ within the space and wavenumber windows which can be defined in the root-mean-square (r.m.s.) sense, consequently leading to a localization which is also expressed in the mean-square sense. The information is then localized with the wavelet transform within a *space window* given by

$$[b + ax^* - a\Delta_\psi, \quad b + ax^* + a\Delta_\psi], \tag{23}$$

where x^* is the center and Δ_ψ is the r.m.s. extent (or radius) of the mother wavelet. In a similar way, the wavelet transform is seen to give localized information in the wavenumber domain within a *wavenumber window* given by

$$\left[\frac{\kappa^*}{a} - \frac{\Delta_{\tilde{\psi}}}{a}, \frac{\kappa^*}{a} + \frac{\Delta_{\tilde{\psi}}}{a} \right], \tag{24}$$

where $\tilde{\psi}(\kappa)$ is the Fourier transform of the mother wavelet and, as before, κ^* is the center and $\Delta_{\tilde{\psi}}$ is the r.m.s. bandwidth (or radius) of the Fourier transform of this mother wavelet.

The quantities Δ_ψ and $\Delta_{\tilde{\psi}}$ also defines space and wavenumber resolutions, associated with a particular wavelet. These resolutions satisfy the uncertainty principle [19]:

$$\Delta_\psi \Delta_{\tilde{\psi}} \geqslant \tfrac{1}{2}. \tag{25}$$

The squared norm of the Fourier transform given by $|\tilde{f}(\kappa)|^2$ is known to lead to a continuous representation of the energy density distribution of $f(x)$ in the wavenumber domain, known as a *spectrogram*. The energy density is thus obtained only as a function of κ. To obtain an energy density distribution of the function in the space–wavenumber plane, a similar quantity can be defined in the case of the wavelet transform as a squared norm given by

$$|(W_\psi f)(b, a)|^2 \tag{26}$$

and this quantity can be referred to as a *scalogram* [20]. The resolution capabilities of the scalogram depend on the analyzed wavenumber, as presented before. The shape of the wavelet ψ and of its Fourier $\tilde{\psi}$ obviously determines a weighting for the localization obtained in both domains. Following equations (23) and (24), the energy is distributed into space and wavenumber windows in the mean-square sense depending on the parameters b and a.

Considering the above, it is first proposed in this section that the squared norm of the wavelet transform of the beam-displacement field, $|(W_\psi w)(b, a)|^2$, can *observe* the contribution of this local displacement field to the total vibratory energy [15]. It is next proposed that the quantity given by

$$\omega_0^3 \left| \frac{2\pi}{\sqrt{|a|}} (W_\psi w)(b, a) \right|^2 \tag{27}$$

can be used to represent the acoustic power radiated by the beam if the parameter a is chosen such that the wavelet transform gives localized energy information in the supersonic region of the wavenumber spectrum. In other words, the choice of the parameter a as well as the use of the multiplying factor ω_0^3 are such that equation (27) mimics the exact expression of the radiated power (10). It is further assumed that a single component in the b-axis is sufficient to represent the energy in the supersonic region. Therefore, the parameter b is set to 0, implying that the wavelet is always centered on the beam.

In the following, due to its simplicity, the Morlet wavelet will be chosen as the mother wavelet even if, rigorously, this wavelet is only numerically admissible, i.e., only numerical reconstruction of $f(x)$ from its wavelet transform is possible. The Morlet wavelet $\psi_G(x)$ is defined as the modulated Gaussian window is given by

$$\psi_G(x) := \frac{1}{2\sqrt{\pi\alpha}} \mathrm{e}^{-\mathrm{i}2\pi(x+3\cdot5)} \mathrm{e}^{-x^2/4\alpha}, \tag{28}$$

where α will be chosen in order to meet special requirements, as shown later. The following centers and radii are easily obtained for the Morlet wavelet:

$$x^* = 0, \qquad \Delta_\psi = \sqrt{\alpha}, \qquad \kappa^* = -2\pi, \qquad \Delta_{\tilde{\psi}} = \frac{1}{2\sqrt{\alpha}}. \tag{29–32}$$

It has been shown [15] that the following relation between the parameter a and the angular frequency ω_0 allows the wavelet transform to localize the energy in the supersonic region of the wavenumber spectrum at frequency ω_0:

$$a = \frac{c}{\omega_0}\frac{\kappa^*}{\gamma}, \tag{33}$$

where a parameter $0{\cdot}5 \leqslant \gamma \leqslant 1$ is used to ensure that, considering the center specified for the window, its width will not cause the window to exceed the supersonic region. Therefore, a design criterion for the Morlet wavelet can be obtained under these conditions:

$$\alpha = \frac{1}{16\pi^2}\frac{\gamma^2}{(1-\gamma)^2}. \tag{34}$$

In the preceding, the wavelet approach was presented using one-wavelet transform. However, in order to cover completely both space and wavenumber domains, i.e., the entire beam and the entire supersonic region, a few wavelet transforms have to be used and thus, a few wavelets in the wavenumber domain, each of them having $b = 0$ and each of them reconstructing the energy in a given subregion of the supersonic region, and then summing all these contributions. By doing so, the *wavenumber window* of each wavelet is of limited extent and, therefore by equation (25), the corresponding spatial extent is larger and then more appropriate to cover the entire beam. The wavelet transforms are performed on the same displacement field but using different mother wavelets, each of them using a different relation between the parameter a and the acoustic frequency (equation (33)) and consequently, a different design criteria α (equation (34)). The approximation using these multiple wavelet transforms then takes the form

$$\Pi^{wavelets} \approx \omega_0^3 \sum_{i=1}^{n} \left| \frac{2\pi}{a_i} \int_{-\Lambda a_i}^{\Lambda a_i} w(x)\,\overline{\psi_{G_i}\left(\frac{x}{a_i}\right)}\,\mathrm{d}x \right|^2, \tag{35}$$

where a_i and ψ_{G_i} are associated with the ith wavelet transform, n is the number of wavelet transforms employed and $[-\Lambda, \Lambda]$ is the region outside which the mother wavelet has negligible values. The scale parameters are given in this case by

$$a_i = \frac{c}{\omega_0}\frac{2n}{2i-1}\kappa^*, \quad i = 1, \ldots, n, \tag{36}$$

while the design criterion for each mother wavelet is given by

$$\alpha_i = \frac{(2i-1)^2}{16\pi^2}, \quad i = 1, \ldots, n. \tag{37}$$

For the baffled beam, the Morlet wavelet can thus be considered to be spatially confined and rewritten as a discrete sum, with $b = 0$ and six displacement estimation points:

$$\Pi^{wavelets} \approx \omega_0^3 \sum_{i=1}^{n} \left| \frac{2\pi}{a_i} \sum_{j=1}^{6} w_j\,\overline{\psi_{G_i}\left(\frac{x_j}{a_i}\right)}\,\Delta x \right|^2, \tag{38}$$

where the displacement values w_j are obtained from strain values using a finite differences scheme, for example. This approach is thus presented as an alternative to the Fourier

transform and the integral, as presented in equation (10), which have to be used for each frequency component. In fact, the proposed approximation of the radiated acoustic power only requires *very few* wavelet transforms to approximate the radiated acoustic power *over the complete frequency range*. Indeed, the resulting components are expressed in terms of the parameter a and a mapping to the frequency domain (ω_0) exists and is given by equation (36). The net computational gain obtained using the wavelet approximation over the Fourier approach is thus dependent on the number of frequency components where the radiated acoustic power is to be evaluated.

4. EXPERIMENTAL VALIDATION OF THE OPTIMIZED APPROACHES

The use of the optimized approaches is assessed through a comparison with the reference finite differences approach using experimental measurements.

4.1. EXPERIMENTAL SET-UP

The experimental set-up used for the validation consists of a simply supported baffled beam onto which, in addition to two piezoelectric patches, a set of PVDF sensors are bonded. The following sections describe the details of the experimental implementation.

4.1.1. *Mechanical set-up*

A simply supported thin beam is mounted in a baffle, as schematically presented in Figure 1. Four PVDF sensors and two piezoceramic (PZT) patches are glued to the beam and located as shown in Figure 2. The beam is excited at a single frequency by a Hewlett-Packard 3245A signal generator and a *Bruel and Kjaer* 4810 shaker between 60 Hz and 1 kHz to produce the primary disturbance vibratory field. The characteristics of the mechanical components are presented in Table 1.

4.1.2. *Sensors and actuators*

The PVDF sensors are used to measure the strain at four discrete points. Each of these sensors is tailored with the same dimension, shown in Table 1. Considering the frequency range of interest and the modal behavior of the beam used in this work, the spatial extent of the PVDF sensors is small enough (as compared to structural wavelength) that a local strain measurement is obtained. A conductive adhesive transfer tape (3M) is used to bond the sensors to the beam. The quantity measured by the PVDF sources is in fact the integral

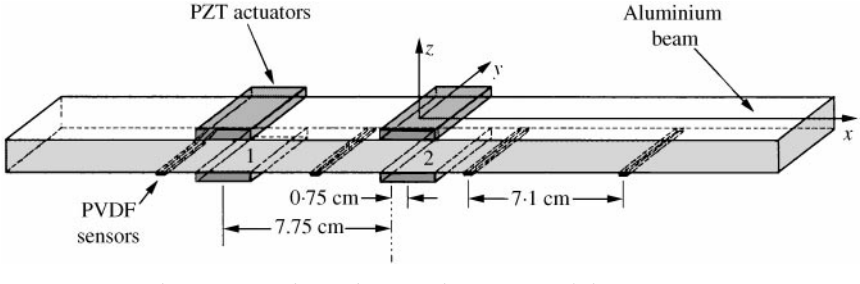

Figure 2. Experimental set-up: the sensors and the actuators.

TABLE 1

Components characteristics

	Beam	Sensors	Actuator(s)
Material	Aluminum	PVDF AMP Inc., AMP 028 CN	PZT Piezo Systems Inc., PSI-5A-S4-ENH
x dimension (m)	0·355	0·0035	0·025
y dimension (m)	0·0252	0·0252	0·0252
Young's modulus E (GPa)	67	2	66
Thickness h (m)	0·003	0·000028	0·000254
Poisson's ratio v	0·3	—	0·29
Density ρ (kg/m^3)	2710	3400	7800
Piezoelectric strain constant d_{31} (m/V)	—	$2{\cdot}3 \times 10^{-11}$	$1{\cdot}9 \times 10^{-10}$

of the strain over the surface of each sensor:

$$q = -(h_b + h_{PVDF}) l_y e_{31} \int_{l_{PVDF}} \varepsilon_x(x)\,\mathrm{d}x, \tag{39}$$

where l_{PVDF} and h_{PDVF} are the length and the thickness of the PVDF, respectively, and e_{31} is the piezoelectric stress constant (the piezoelectric stress constant $\mathbf{e}$ is related to the piezoelectric strain constant $\mathbf{d}$ by $\mathbf{e} = \mathbf{E}_p\mathbf{d}$, where $\mathbf{E}_p$ is the Young's modulus of the piezoelectric). The charge signals q are converted to voltages using in-house charge amplifiers. These signals are then filtered by Rockland 852 anti-aliasing filters at 1 kHz and a sampling frequency of 3 kHz is used.

The actuators used for the control consist of two sets of colocated piezoceramics mounted on opposite faces of the beam and driven by a voltage such that the mechanical action of both piezoceramics is out of phase with respect to each other, i.e., one piezoceramic extends when the other contracts. It has been shown that in such a configuration, the action of each piezoceramic patch is equivalent to the application of two moments at the edges of the patch [21]. Moreover, these moments are proportional to the voltage applied to the piezoceramic patch. The first piezoceramic patch is located at $x = 0{\cdot}0075$ m while the second patch is located at $x = -0{\cdot}0775$ m. The control signals fed to the actuators are filtered by a Rockland 2382 anti-aliasing filter at 1 kHz and amplified using a PCB Piezotronics AVC 790 high-voltage amplifier.

4.1.3. *Controller configuration*

A feedforwad configuration was used for the controller together with a filtered-X least-mean-square (LMS) algorithm. The cost function used in the experimental validation is the radiated acoustic power approximated from structural measurements using the three previous approaches. In order to allow for the calculation of this cost function, the control algorithm is divided into two parts: the control part (real-time task) and the optimization part (idle processor time task), as shown in Figure 3. An off-line adaptation of a correction to the control filter is performed during the idle processor time and added to the control filter when possible. In practice, for the cases studied in this paper, this update takes less than 0·5 s. FIR filters are used for the control path model and the control filter. The control path model is identified off-line using 1024 coefficients while the control filter uses four

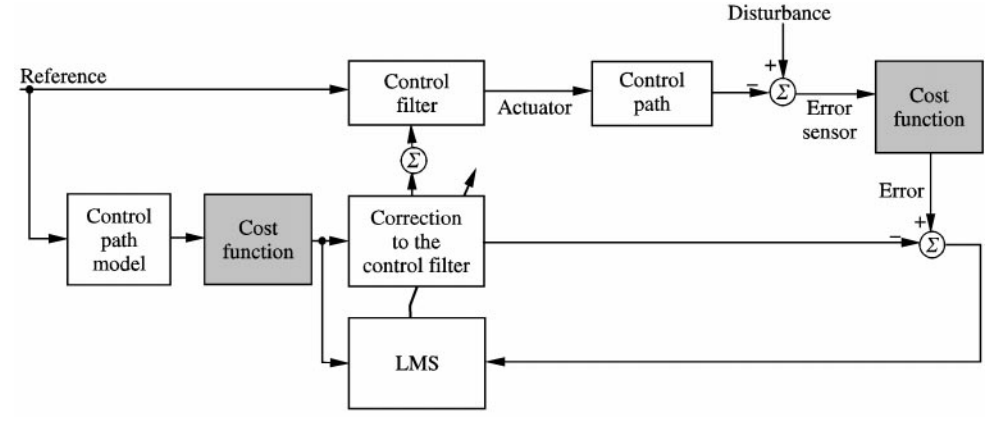

Figure 3. Off-line controller configuration.

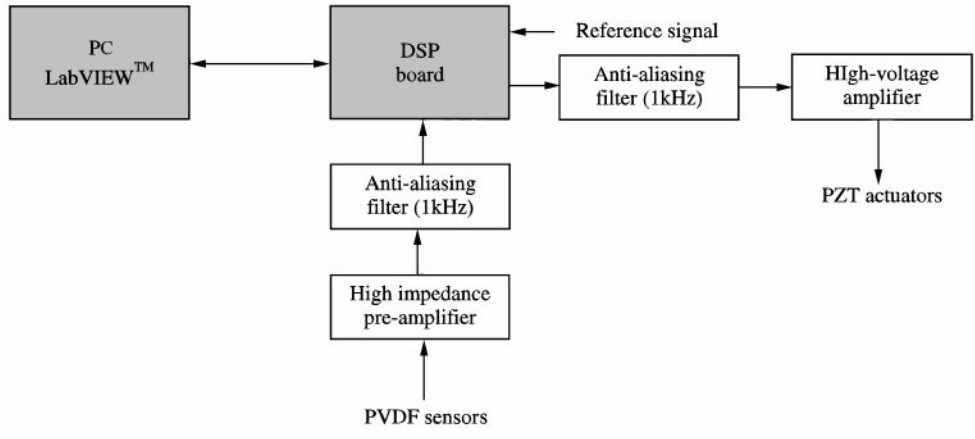

Figure 4. Schematic representation of the control system.

coefficients. The reference signal used by the feedforward controller is taken directly from the signal generator.

Figure 4 presents the complete control system with the PVDF sensors and the PZT actuators. The controller operates on a Spectrum board equipped with a TMS 320C31 DSP. The National Instruments LabVIEW environment is used to download the code into the DSP and monitor the controller operation.

4.1.4. *Control performance metrics*

A set of seven TMS ICP 130M01/P10 microphones located on a hemisphere in front of the beam as well as a Poltype OFV 2600-302 laser vibrometer are used to monitor the control performance of the approaches, through a Hewlett-Packard 3566A spectrum analyzer. In this respect, the radiated acoustic power is obtained from the pressure measurements by (equation (8))

$$\Pi = \frac{1}{2\rho_0 c}\frac{2\pi R^2}{7}\sum_{i=1}^{7}|p_i(R,\theta_i,\varphi_i)|^2, \tag{40}$$

where $R = 0{\cdot}52$ m, while the mean-square velocity $\langle \dot{w}^2 \rangle$ is obtained from nine equally spaced velocity measurements on the beam by

$$\langle \dot{w}^2 \rangle = \frac{1}{4l_x} \sum_{i=1}^{9} |\dot{w}_i|^2 \Delta x. \tag{41}$$

The measurements were conducted in a semi-anechoic room having a cut-off frequency of 100 Hz.

4.2. EXPERIMENTAL RESULTS

Experimental results are presented to assess the proposed optimized approaches for the use of strain sensing in active structural acoustic control. The use of strain measurements for the estimation of radiated acoustic power is first experimentally assessed through the reference finite differences approach. The control performance obtained using this estimation is also presented. The control performance of both optimized approaches is then presented and compared with the control performance obtained using the reference approach. A comparison of the finite differences approach with an approach involving the minimization of the sum of the strain measurements has been presented before by the authors [22].

4.2.1. *Finite differences approach*

The first experimental validation concerns the ability of the finite differences scheme to reconstruct the displacement field from the strain field and to provide an adequate estimate of the radiated acoustic power. The estimation of this radical acoustic power from velocity (and hence, displacement) measurements given by the laser vibrometer and from strain measurements is compared in Figure 5, together with the radiated acoustic power obtained from pressure measurements. This figure shows that the reconstruction scheme tends to

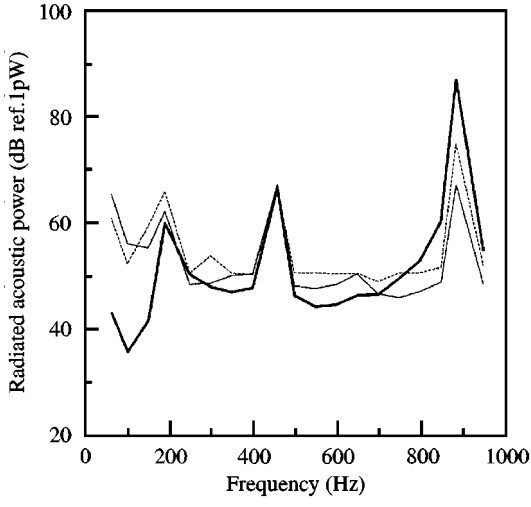

Figure 5. Radiated acoustic power obtained from displacement field reconstruction from strain measurements and as calculated from pressure and velocity measurements: - - -, from pressure measurements; —, from velocity measurements; ——, from strain measurements.

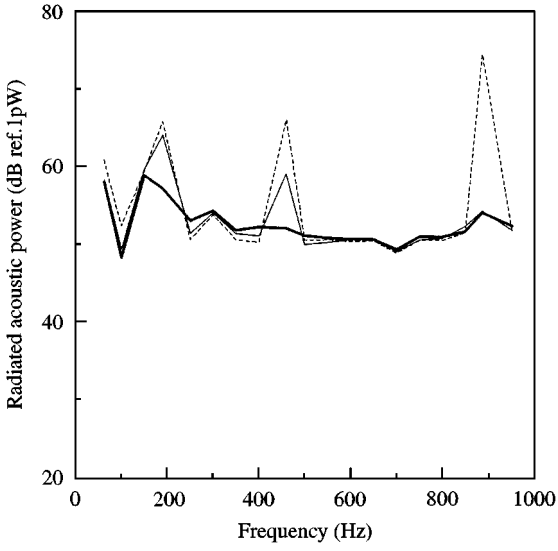

Figure 6. Effect of the number of actuators for the control of the radiated acoustic power using the finite differences approach: - - -, before control; ——, control one actuator; ———, control two actuators.

underestimate the radiated acoustic power at low frequency, which can be explained by a poor signal-to-noise ratio involved in the finite differences scheme in this region. At high frequency, an insufficient number of sensors translates into a poor estimate of the radiated acoustic power.

Control results are now presented in Figure 6 with the effect of the number of actuators used for the control in the finite differences approach. It appears that an increase in the number of actuators is beneficial to the control performance at low frequency. A possible explanation to this could come from the control objective which requires the restructuring of the vibration pattern instead of the direct attenuation of the vibration levels.

4.2.2. *Direct approach*

All the results presented in the next two sections use two actuators for the control. The control performance of the direct approach is first compared to the control performance of the finite differences approach. The radiated acoustic power obtained from pressure measurements after control with these approaches is presented in Figure 7. The performance of the direct approach is noticeable, considering that it involves a lower computational burden. This could translate into a faster adaptation to variations in the statistics of the disturbance signal. The effect of both approaches on the mean-square velocity is presented in Figure 8, which reveals that the direct approach aims more at minimizing the vibrations of the structure. This is more apparent on the radiation efficiency σ, defined as

$$\sigma = \frac{\Pi}{4\rho_0 c l_x l_y \langle \dot{w}^2 \rangle} \tag{42}$$

which is presented in Figure 9.

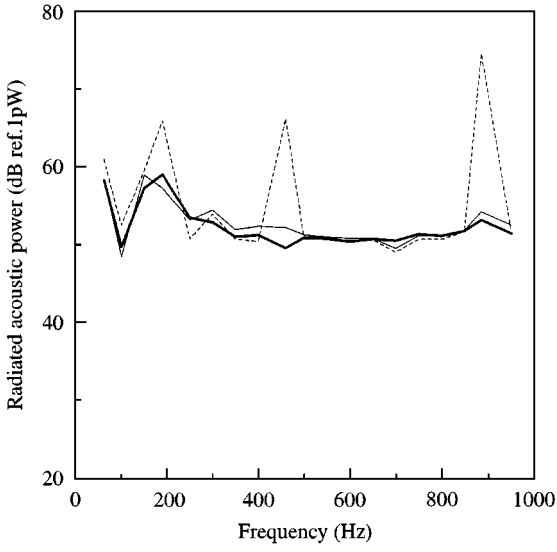

Figure 7. Comparison of the radiated acoustic power as controlled using the finite differences approach and the direct approach: - - -, before control: ——, finite differences: ———, direct approach. Two actuators are used.

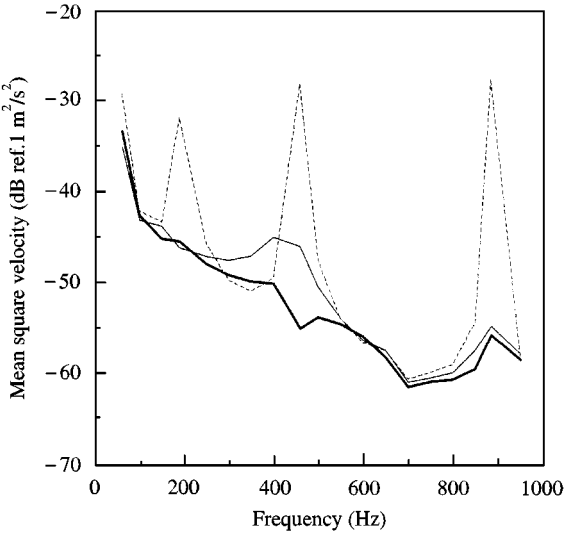

Figure 8. Comparison of the mean-square velocity as obtained after the control of the radiated acoustic power using the finite differences approach and the direct approach: - - -, before control: ——, finite differences: ———, direct approach. Two actuators are used.

The reconstruction problem noticed at low frequency in the finite differences approach (see Figure 5) is further illustrated in Figure 10 which shows the cost function in the direct and finite differences approaches after the control has been applied. The curves presented in this figure show that the finite differences approach provides a biased estimate of the radiated acoustic power, especially at low frequency, which results in a slightly smaller acoustic power reduction.

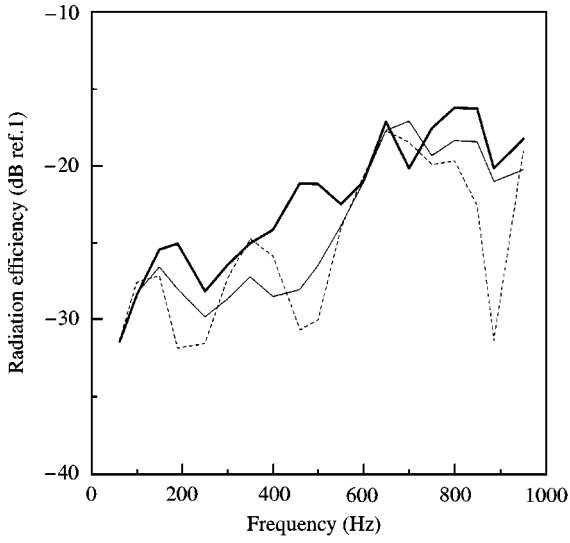

Figure 9. Comparison of the radiation efficiency as obtained after the control of the radiated acoustic power using the finite differences approach and the direct approach: - - -, before control; ——, finite differences; ———, direct approach. Two actuators are used.

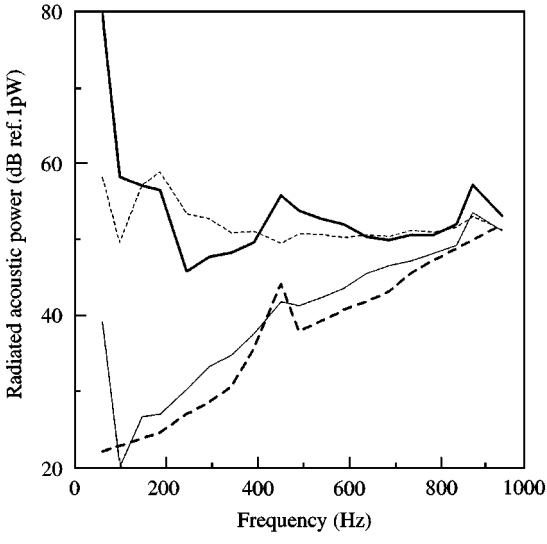

Figure 10. Comparison of the radiated acoustic power as measured and as obtained from the cost function after the control using the finite differences approach, the direct approach and the wavelet approach: - - -, from pressure measurements; —— cost function finite differences: ———, cost function direct approach; - - -, cost function wavelet approach. Two actuators are used.

4.2.3. *Wavelet approach*

The second optimized approach to be compared to the finite differences approach is the wavelet approach. The wavelet approach is of interest because it allows a fast approximation of the radiated acoustic power without making, by itself, any assumptions on the boundary conditions. For these experimental results, $n = 4$ wavelet transforms are

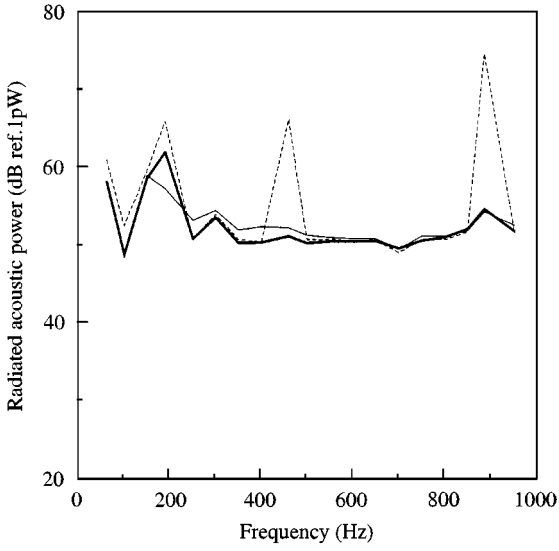

Figure 11. Comparison of the radiated acoustic power as controlled using the finite differences approach and the wavelet approach: - - -, before control: ——, finite differences; ———, wavelet approach. Two actuators are used.

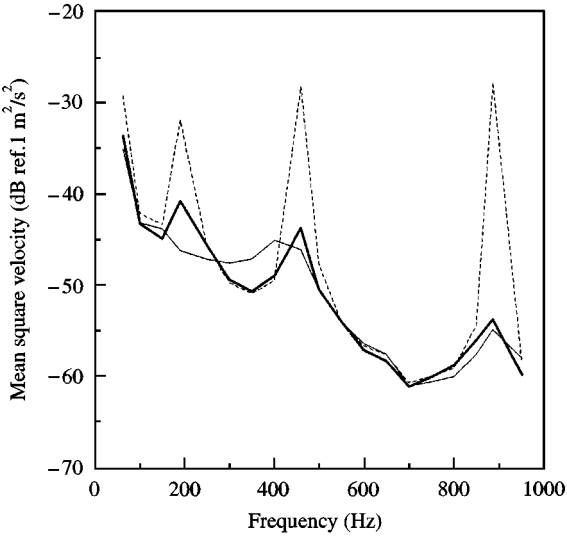

Figure 12. Comparison of the mean-square velocity as obtained after the control of the radiated acoustic power using the finite differences approach and the wavelet approach: - - -, before approach: ——, finite differences; ———, wavelet approach. Two actuators are used.

used to estimate the radiated acoustic power. The comparison is presented in Figures 11–13. The good control performance of the wavelet approach is very encouraging since it could provide a very efficient tool for the broadband control of the acoustic power radiated from structures. These results confirm the optimal control results obtained previously [15]. Moreover, as seen on the mean-square velocity and on the radiation efficiency, the control mechanism involved in the wavelet approach seems to resemble the control mechanism

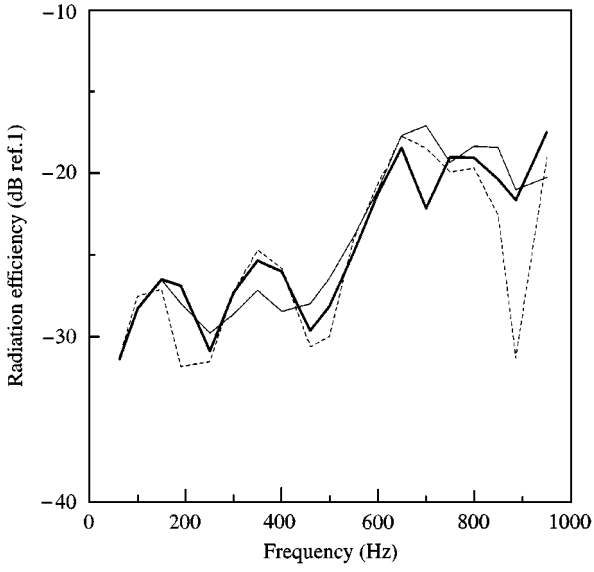

Figure 13. Comparison of the radiation efficiency as obtained after the control of the radiated acoustic power using the finite differences approach and the wavelet approach: - - - , before control; ——, finite differences; ———, wavelet approach. Two actuators are used.

involved in the radiated acoustic power control as estimated by the finite differences scheme. It should be noted that the wavelet approach also suffers from reconstruction problems at low frequency (see section 4.2.1) as it is based on the use of a reconstructed displacement field; this is illustrated in Figure 10.

5. CONCLUSIONS

Two optimized approaches were presented and experimentally validated using piezoelectric discrete strain sensors. A baffled simply supported beam was used for the validation. The first optimized approach was presented to allow the evaluation of the radiated acoustic power directly from the strain measurements, without the need for a reconstruction scheme. The second optimized approach was presented to accelerate the evaluation of the radiated acoustic power through an estimate based on the wavelet transform.

The experimental set-up was presented, together with some details on the real-time implementation of the approaches. Pressure and velocity measurements were made to better understand and illustrate the control mechanisms involved in the different approaches.

The experimental results show that the reference finite differences approach suffers from a poor signal-to-noise ratio at low frequency, but still offers a very interesting control performance over the whole frequency range. These results confirm previous analytical results indicating a reconstruction problem at low frequency. The results also show that the optimized approaches perform very well in attending the radiated acoustic power under control. The direct approach seems to provide a more realistic representation of the radiated acoustic power to the controller. This approach is however restricted to cases where boundary terms can be neglected. Being applicable to more general structures, the wavelet approach represents an interesting alternative as it appears to behave like the

complete radiated acoustic power approach. This indicates that this approach is expected to be more efficient for planar structures especially if broadband control is required. Fast algorithms involving filter banks for the wavelet transform can be used. Because they use discrete sensors, all the approaches can be extended to two-dimensional structures, preserving the distinction between the wavenumber components, still allowing for a wavenumber approach.

Work on the extension of the approaches to two-dimensional structures with different boundary conditions is currently in progress. The exploitation of spatial localization property of the wavelet transform is also being investigated.

ACKNOWLEDGMENT

This work was supported by the Natural Sciences and Engineering Research Council (NSERC), Canada.

REFERENCES

1. S. J. ELLIOTT and P. A. NELSON 1993 *IEEE Signal Processing Magazine* **10**, 12–35. Active noise control.
2. C. R. FULLER 1990 *Journal of Sound and Vibration* **136**, 1–15. Active control of sound transmission/radiation from elastic plates by vibration inputs: I. Analysis.
3. Y. C. PARK and S.D . SOMMERFELDT 1997 *Journal of the Acoustical Society of America* **101**, 350–359. Global attenuation of broadband noise fields using energy density control.
4. J. P. MAILLARD and C. R. FULLER 1994 *Journal of the Acoustical Society of America* **95**, 3252–3261. Advanced time domain wave-number sensing for structural acoustic systems. Part I. Theory and design.
5. J. P. MAILLARD and C. R. FULLER 1994 *Journal of the Acoustical Society of America* **95**, 3262–3272. Advanced time domain wave-number sensing for structural acoustic systems. Part II. Active radiation control of a simply supported beam.
6. J. P. MAILLARD and C. R. FULLER 1995 *Journal of the Acoustical Society of America* **98**, 2613–2621. Advanced time domain wave-number sensing for structural acoustic systems. Part III. Experiments on active broadband radiation control of a simply supported plate.
7. C. GUIGOU, A. BERRY, F. CHARETTE and J. NICOLAS 1996 *Acta Acustica* **82**, 772–783. Active control of finite beam volume velocity using shaped PVDF sensor.
8. C. GUIGOU, A. BERRY and F. CHARETTE 1994 *Proceedings of the ASME Winter Annual Meeting, Chicago*, 247–255. Active control of plate volume velocity using shaped PVDF sensor.
9. Y. GU and C. R. FULLER 1993 *Journal of the Acoustical Society of America* **93**, 337–345. Active control of sound radiation from a fluid-loaded rectangular uniform plate.
10. P. MASSON, A. BERRY and J. NICOLAS 1997 *Journal of the Acoustical Society of America* **102**, 1588–1599. Active structural acoustic control using strain sensing.
11. C. R. FULLER and R. A. BURDISSO 1991 *Journal of Sound and Vibration* **148**, 355–360. A wavenumber domain approach to the active control of structure-borne sound.
12. S. D. SOMMERFELDT 1993 *Proceedings of the Second Conference on Recent Advances in Active Control of Sound and Vibration*, 929–940. Active wavenumber control of acoustic radiation from a plate.
13. R. L. CLARK and C. R. FULLER 1992 *Journal of the Acoustical Society of America* **91**, 3321–3329. Modal sensing of efficient acoustic radiators with polyvinylidene fluoride distributed sensors in active structural acoustic control approaches.
14. S. D. SOMMERFELDT and B. L. SCOTT 1994 *Proceedings of Noise-Con* 94, 279–284. Estimating acoustic radiation using wavenumber sensors.
15. P. MASSON A. BERRY and P. MICHEAU 1998 *Journal of the Acoustical Society of America* **104**, 1453–1465. A wavelet approach to the active structural acoustic control.
16. A. BERRY, J. L. GUYADER and J. NICOLAS 1990 *Journal of the Acoustical Society of America* **88**, 2792–2802. A general formulation for the sound radiation from rectangular, baffled plates with arbitrary boundary conditions.

17. R. L. CLARK and C. R. FULLER 1991 *Proceedings of the Conference on Recent Advances in Active Control of Sound and Vibration*, 507–524. Active structural acoustic control with adaptive structures including wavenumber considerations.
18. F. FAHY 1985 *Sound and Structural Vibration. Radiation, Transmission and Response*. New York: Academic Press.
19. C. K. CHUI 1992 *An Introduction to Wavelets. Series on Wavelet Analysis and its Applications*. New York: Academic Press.
20. O. RIOUL and P. FLANDRIN 1992 *IEEE Transactions on Signal Processing* 1746–1757. Time-scale energy distributions: a general class extending wavelet transforms.
21. E. K. DIMITRIADIS, C. R. FULLER and C. A. ROGERS 1991 *ASME Journal of Vibration and Acoustics* **113**, 100–107. Piezoelectric actuators for distributed vibration excitation of thin plates.
22. P. MASSON, A. BERRY and A. MORIN 2000 *Journal of Intelligent Material Systems and Structures* **10**, 71–82. Experiments on the use of fiber-optic strain sensors in active structural acoustic control.